

Intermediate energy four-body breakup calculations for ^{22}C

Y. Kucuk^{1,2,*} and J. A. Tostevin²

¹*Department of Physics, Giresun University, 28100-Giresun, Turkey*

²*Department of Physics, Faculty of Engineering and Physical Sciences,
University of Surrey, Guildford, Surrey GU2 7XH, United Kingdom*

(Dated: June 19, 2021)

The heaviest particle-bound carbon isotope, ^{22}C , is thought to have a Borromean three-body structure. We discuss and compare four-body, i.e. three-body projectile plus target, reaction model calculations of reaction cross sections for such systems that use the fast adiabatic approximation. These methods are efficient and well-suited for quantitative analyses of reactions of neutron-rich nuclei with light target nuclei at secondary beam energies of ≈ 300 MeV/nucleon, as are now becoming available. We compare the predictions of the adiabatic model of the reaction both without and when including the additional eikonal approximation that has been used extensively. We show that the reaction cross section calculations have only limited sensitivity to the size and structure of ^{22}C and that the differences arising from use of the eikonal approximation of the reaction mechanism are of a similar magnitude.

PACS numbers: 24.50.+g, 25.60.-t, 25.70.-z, 27.30.+t

I. INTRODUCTION

Reaction and interaction cross sections of light neutron- and proton-rich projectiles with light target nuclei have been used extensively as an inclusive observable with sensitivity to projectile size and binding. Calculations of the elastic scattering, reaction and breakup observables of weakly-bound two-neutron-halo nuclei, the ground states of which can be modelled using three-body-model wave functions, is a four-body reaction problem. As was shown in previous three- and four-body analyses of the reaction cross sections for weakly-bound nuclei, the treatment of breakup degrees of freedom is essential to obtain a quantitative description of the reaction observables. Practical calculations that treat the few-body structure of the projectile explicitly are now possible. For example, at high energies, of order 800 MeV/nucleon, the eikonal (Glauber) theory has been employed [1, 2] that provides an efficient approximate methodology. Counter to ones intuition, the inclusion of strongly-coupled breakup channels, that remove flux from the elastic channel, actually resulted in calculated reaction cross sections that were smaller than those obtained using simpler (no-breakup) one-body density-based models, which overestimate the contribution to the cross sections from the dilute halo of one or more weakly-bound neutrons [1, 2]. This is also expected to be the case for reactions of the heaviest particle-bound carbon isotope, ^{22}C , for which first measurements are now possible, see e.g. [3]. That data set suggested an enhanced ^{22}C reaction cross section on a proton target at relatively low energy and the authors used a simplified reaction model to infer a very large root-mean-squared (rms) matter radius for ^{22}C . Inclusive measurements of

Coulomb dissociation of ^{22}C on a heavy (Pb) target [4] and of fast nucleon removal on a light (C) target [5] have also recently been performed at RIKEN at energies in excess of 200 MeV/nucleon, also displaying enhanced reaction yields characteristic of weak binding.

In this paper we exploit the coupled-channels adiabatic approach of Christley *et al.* [6] for (four-body) model calculations of reaction cross sections, σ_R . We compare these calculations with the adiabatic plus eikonal four-body dynamical approach [1, 2] that makes additional approximations. Our primary objectives are twofold. (i) To quantify the sensitivity of the σ_R to the structure assumed for this weakly-bound dripline (and Borromean) system and clarify the breakup channels of most importance. Since the adiabatic method is computationally more efficient, a knowledge of this convergence may offer insight into the likely model space(s) needed for higher-energy calculations using e.g. the coupled discretized continuum channels approach [7, 8]. (ii) To quantify the differences between the σ_R calculations that use and do not use the additional eikonal approximation(s) to the adiabatic model. To do this we explore the ^{22}C nucleus ground-state wave function within a core plus two-valence neutron ($^{20}\text{C}+n+n$) three-body framework [9] and the reaction dynamics using the four-body adiabatic model, see [6]. The converged results of this approach are compared with calculations that use the same ^{22}C wave functions and optical model interactions but which make the additional eikonal approximation to the reaction dynamics of the four-body problem: as have been used previously [1, 2]. This paper supersedes the brief report of preliminary results of the present study of Ref. [10].

*Present address: Akdeniz University, Antalya, Turkey

II. PROJECTILE THREE-BODY MODEL

The nucleus ^{22}C and its neutron-unbound subsystem ^{21}C remain poorly understood. Both the two-neutron separation energy from ^{22}C and the ground-state energy of ^{21}C are poorly determined. The 2003 mass evaluation [11] gives $S_{2n}(22) = 0.4(8)$ MeV and $S_{1n}(21) = -0.3(6)$ MeV, both with large uncertainties. A recent direct mass measurement places a limit of $S_{2n}(22) = -0.140(460)$ MeV [12], however, since ^{22}C is known to be bound, this might be interpreted as $S_{2n}(22) < 0.32$ MeV [13]. Irrespective of such details, ^{22}C is certainly bound (unbound) and thus ^{22}C has a Borromean, $^{20}\text{C}+n+n$ three-body character and is very interesting structurally. The shell-model suggests that this $N = 16$ nucleus will, predominantly, be described by a $\nu[1d_{5/2}]^6 [2s_{1/2}]^2$ closed neutron sub-shell configuration. The expectation is therefore that ^{22}C will have an extended, predominantly s -wave two-neutron-halo wave function leading to large reaction, nuclear, and Coulomb dissociation cross sections in its collisions with a target nucleus.

A very recent analysis of new measurements of (inclusive) neutron removal reactions from the most neutron-rich carbon isotopes [5], also made at the RIBF, RIKEN at 240 MeV per nucleon, is broadly consistent with this shell-model picture. The $^{22}\text{C}(-1n)$ data suggest a large spectroscopic factor (of ≈ 1.4) for $2s_{1/2}$ neutron removal to an unbound $^{21}\text{C}(1/2^+)$ ground state, which subsequently decays by neutron emission to ^{20}C . These data are also consistent with (though not highly sensitive to) the $S_{2n}(22)$ and $S_n(21)$ of the 2003 mass evaluation [11] and the $S_{2n}(22)$ limit of the recent direct mass measurement [12].

This same set of measurements [5] also identifies a non-negligible $\nu[2s_{1/2}]^2$ component in the (isolated) $^{20}\text{C}(0^+)$ ground-state, manifest as population of the $^{19}\text{C}(1/2^+)$ ground-state in the neutron removal reaction from ^{20}C projectiles. This complication and the finer details of the structure of the ^{20}C core within ^{22}C will not be explored further in this paper.

A. Model wave function

Here we treat ^{22}C using the three-body model, shown schematically in Figure 1, as a $^{20}\text{C}(0^+)$ core+ $n+n$ system. Related ^{22}C structure studies can be found in Refs. [14, 15], on which we comment. The core is assumed to have a filled $\nu[1d_{5/2}]^6$ sub-shell. The n - n and nn -core relative orbital angular momenta are ℓ_1 and ℓ_2 in our chosen (T-basis) Jacobi coordinate set \mathbf{r} and $\boldsymbol{\rho}$, respectively.

The projectile's ground state wave function (and the structure of the wave function in the breakup channel with total angular momentum IM_I) is written, in general, as a sum of individual angular momentum compo-

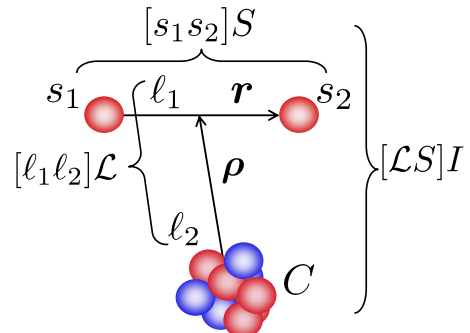


FIG. 1: (Color online) Schematic representation of the angular momentum decomposition and the angular momentum couplings (in the Jacobi T-basis) used for the description of the $^{20}\text{C}(0^+)$ core+ $n+n$ Borromean three-body projectile in its ground and (continuum) excited states. In the case of the ^{22}C ground state, with $I^\pi = 0^+$, $\mathcal{L} = S$ and $[s_1 s_2]S = 0, 1$ and, with $[\ell_1 \ell_2]\mathcal{L}$, $\mathcal{L}^\pi = 0^+$ or 1^+ .

nents

$$\Phi_{IM_I}(\boldsymbol{\rho}, \mathbf{r}) = \sum_{\ell_1 \ell_2 \mathcal{L} S} [[\ell_1 \otimes \ell_2]_{\mathcal{L}} \otimes S]_{IM_I} \frac{U_{[[\ell_1 \ell_2]_{\mathcal{L}} S] I}(\boldsymbol{\rho}, \mathbf{r})}{\rho r}, \quad (1)$$

only a small number of which are expected to have significant probabilities, as discussed below. The two-neutron configurations are thus $(2S+1)\ell_1$. For the ^{22}C ground state $I^\pi = 0^+$ and thus $\mathcal{L} = S$ and, given that $[\ell_1 \ell_2]\mathcal{L}$, then $\mathcal{L}^\pi = 0^+$ or 1^+ .

B. Three-body model parameters and results

To solve for the three-body wave function we use the Gogny, Pires and De Tourreil (GPT) interaction [16] for V_{nn} . The neutron- ^{20}C core interactions V_{n20}^ℓ are described by Woods-Saxon plus spin-orbit interactions. For all ℓ_j -states we use radius and diffuseness parameters 1.25 fm and 0.65 fm, respectively, and a spin-orbit strength $V_{so} = 6.3$ MeV. This (derivative Woods-Saxon) neutron- ^{20}C spin-orbit potential is defined according to the convention of Becchetti and Greenlees [17].

The depth of the central d -wave neutron-core interaction, $V_0^{\ell=2} = 42.0$ MeV, was chosen to bind the neutron+ ^{20}C $1d_{5/2}$ state (by 2.3 MeV) while the $1d_{3/2}$ state is unbound by 1.9 MeV. This fixed potential was used for all $n\ell_j$ neutron+ ^{20}C configurations other than the s -wave states. For the s -states this depth is too strong, binding the $2s_{1/2}$ state. The s -state well depth, $V_0^{\ell=0}$, was thus adjusted (reduced) so that the $n+^{20}\text{C}$ $2s_{1/2}$ state is unbound, as expected empirically. This two-body s -state potential depth and the strength, V_{3B} , of an added attractive central hyperradial three-body force,

$$V_{3B}(\varrho) = -V_{3B}/(1 + [\varrho/5]^3), \quad (2)$$

were then used as parameters to generate bound ^{22}C three-body wave functions with a range of three-body energies, allowed by the uncertainty on the evaluated ^{22}C two-nucleon separation energy. We use $V_{3B} = 1.6$ MeV. Each wave function is thus characterised by (a) the position of the $n+^{20}\text{C}$ $s_{1/2}$ virtual state pole (located using a complex k -plane S-matrix search [18]) and its associated scattering length a_0 and (b) its bound three-body energy eigenvalue, $E_{3B} = -S_{2n}$. Even in the absence of the added three-body force V_{3B} , ^{22}C is found to be bound with the potential set used, provided that $a_0 \leq -46$ fm. With $V_{3B} = 0$ and the largest a_0 value, model k5 in Table I, $S_{2n}(22) = 134$ keV.

The parameters of our calculated wave functions and the probabilities for their most important two-neutron configurations are shown in Table I. These are all dominated by the neutron $[\nu 2s_{1/2}]^2$ configuration. These calculations use a maximum hypermomentum $K_{\text{max}} = 45$. The ^{22}C point-nucleon rms matter radii $\langle r^2 \rangle_{22}^{1/2}$ are also shown, computed using $\langle r^2 \rangle_{22} = (20/22)\langle r^2 \rangle_{20} + \langle \varrho^2 \rangle / 22$, where $\langle \varrho^2 \rangle$ is the mean-squared hyperradius [19]. The rms radius of the ^{20}C core, $\langle r^2 \rangle_{20}^{1/2}$, is taken to be 2.913 fm, from the neutron and proton point-particle densities of a Skyrme Hartree-Fock (HF) calculation and the SkX interaction [20]. Given the increased mass of the ^{20}C core in this case, the variations in the theoretical rms radii obtained ($\approx 6\%$) are far more restricted than was obtained e.g. for ^{11}Li ($\approx 30\%$), as were shown in Fig. 4 of Ref. [2]. We note that none of these $[\nu 2s_{1/2}]^2$ dominated wave functions, that have the correct large-distance three-body asymptotics, has an rms radius within the 1σ -error bar on the very large rms radius, 5.4(9) fm, reported from a simplified reaction description of a low-energy σ_R measurement on a proton target [3].

A different set of potential choices was used in Ref. [14], in which the unbound $s_{1/2}$ virtual state was also placed close to the ^{21}C threshold, while the $1d_{3/2}$ state was located at a significantly higher energy. In Ref. [15], similarly to here, the position of the $s_{1/2}$ virtual state was varied (there between 0 and 100 keV), however a very simple contact (δ -function) n-n interaction was used, thus acting only in n-n relative s -waves. Our set of ^{22}C wave functions includes systems with $S_{2n} \approx 70$ keV and less, as was suggested following a recent experimental ^{21}C search and the use of a zero-range three-body model analysis by Mosby *et al.* [13].

III. FOUR-BODY REACTION APPROACHES

We now describe both the coupled channels and eikonal model methodologies used for the four-body calculations of the elastic scattering S-matrix and the reaction cross sections of projectiles (e.g. ^{22}C), described by three-body model wave functions, incident upon a nuclear target. We use and generalise the adiabatic four-body approach as has been discussed previously by Christley *et al.* [6], applied there to study ^{11}Li elastic scattering, and also

the eikonal model, as was discussed previously for elastic scattering in Ref. [21] and for reaction cross sections in Refs. [1, 2] and elsewhere. We do not consider the role of Coulomb dissociation, given our interest in light target nuclei and intermediate energies. The Coulomb interaction, $V_C(R)$, can be included between the centres of mass of the projectile and target.

A. Adiabatic four-body model calculations

A detailed formulation of the adiabatic four-body model, as applied to the elastic scattering of a three-body projectile, was presented by Christley *et al.* [6]. In this work, as there, the three projectile constituents (the neutrons and ^{20}C core) are assumed to interact with the target nucleus through complex, spin-independent optical potentials, with the result that the total spin of the two neutrons, $[s_1 s_2]S$, is a constant of the motion. In addition to the three-body quantum numbers defined in Figure 1, we denote the relative orbital angular momentum between the centers of mass of the composite projectile and the target by L and their separation by \mathbf{R} .

The adiabatic approximation is common to both the coupled channels and the few-body Glauber approaches. It assumes that the projectile (^{22}C) breakup is predominantly to low-energy states in the continuum, and thus that the typical energies associated with the $^{20}\text{C}+n+n$ three-body Hamiltonian $h(\boldsymbol{\rho}, \mathbf{r})$ are small. In practice one assumes it is a good approximation to replace $h(\boldsymbol{\rho}, \mathbf{r})$ by the projectile ground-state energy, $h(\boldsymbol{\rho}, \mathbf{r}) \rightarrow E_{3B}$, in the four-body, $^{22}\text{C}+\text{target}$ Schrödinger equation for $\Psi(\mathbf{R}, \boldsymbol{\rho}, \mathbf{r})$. This energy choice, E_{3B} , ensures that the dominant elastic components of the wave function have the correct channel energy and asymptotic properties. Thus, the adiabatic model solution of the four-body scattering problem, $\Psi^{\text{Ad}}(\mathbf{R}, \boldsymbol{\rho}, \mathbf{r})$, satisfies

$$[E - E_{3B} - T_R - V_C(R)] \Psi^{\text{Ad}} = V(\mathbf{R}, \boldsymbol{\rho}, \mathbf{r}) \Psi^{\text{Ad}}, \quad (3)$$

in which the coordinates $\boldsymbol{\rho}$ and \mathbf{r} that describe the $^{20}\text{C}+n+n$ relative motions enter only as parameters and not dynamically. Here $V(\mathbf{R}, \boldsymbol{\rho}, \mathbf{r}) = V_{n1} + V_{n2} + V_{20}$ is the total interaction between ^{22}C and the target nucleus, i.e. the sum of the two neutron-target and the core-target two-body interactions for a given $\boldsymbol{\rho}$ and \mathbf{r} . For calculations of elastic scattering and/or reaction cross sections, i.e. of the ^{22}C -target elastic S-matrix as a function of L , Eq. (3) must be partial-wave decomposed and solved for all values of ρ and r relevant to the description of the ^{22}C ground-state wave function. As we discuss weakly-bound projectiles, this will involve an extended region of configuration space.

So, for each fixed radial configuration (ρ, r) between the neutrons and the core the collision and excitation of the system is computed by the solution of an adiabatic (single, fixed energy) radial coupled channels set. These coupled radial wave functions, $\chi_{\alpha'\alpha}^J(R, \rho, r)$, involve a chosen set of internal and orbital configurations

TABLE I: Three-body model wave functions for the ground state of $^{22}\text{C}(I^\pi = 0^+)$ calculated using the code EFADDY [9]. The probabilities associated with the dominant two-neutron components $^{(2S+1)}\ell_1(\text{nn})$ of each wave function are shown (see also Fig. 1) as are the calculated ^{22}C point-nucleon matter rms radii, $\langle r^2 \rangle_{22}^{1/2}$, the computed three-body binding energy E_{3B} and the $n+^{20}\text{C}$ $2s_{1/2}$ virtual state scattering length a_0 for each case. Wave functions k1–k4 include an attractive central three-body force in the hyper-radial coordinate, given by Eq. (2), with strength $V_{3B}=1.6$ MeV. For wave function k5, $V_{3B} = 0$.

Model	$V_0^{\ell=0}$ (MeV)	V_{3B} (MeV)	E_{3B} (MeV)	a_0 (fm)	$^1S(\text{nn})$	$^1D(\text{nn})$	$^1G(\text{nn})$	$\langle r^2 \rangle_{22}^{1/2}$ (fm)	$[2s_{1/2}]^2$	$[1d_{3/2}]^2$
k1	33.5	1.6	-0.442	-333.3	0.698	0.234	0.043	3.505	0.931	0.028
k2	33.0	1.6	-0.294	-45.5	0.721	0.213	0.042	3.571	0.927	0.029
k3	32.5	1.6	-0.163	-24.4	0.744	0.193	0.042	3.643	0.923	0.029
k4	32.0	1.6	-0.046	-16.1	0.767	0.174	0.041	3.719	0.919	0.029
k5	33.5	0.0	-0.134	-333.3	0.743	0.191	0.047	3.669	0.939	0.020

$\alpha = \{\beta, L\}$, with $\beta = [\ell_1 \ell_2] \mathcal{L}$. The coupled equations, $[\mathcal{L}L]J$, are with total orbital angular momentum J , with couplings

$$\left[(E - E_{3B}) + \frac{\hbar^2}{2\mu} \left(\frac{d^2}{dR^2} - \frac{L'(L'+1)}{R^2} \right) - V_C(R) \right] \chi_{\alpha'\alpha}^J(R, \rho, r) = \sum_{\alpha''} V_{\alpha'\alpha''}^J(R, \rho, r) \chi_{\alpha''\alpha}^J(R, \rho, r).$$

Here, the radial coupling interactions are $V_{\alpha'\alpha''}^J(R, \rho, r) \equiv \langle \alpha'; J | V(\mathbf{R}, \boldsymbol{\rho}, \mathbf{r}) | \alpha''; J \rangle$, where the bra-ket notation denotes integration over the angular coordinates of \mathbf{R} , $\boldsymbol{\rho}$ and \mathbf{r} ; see also. Eq. (13) of Ref. [6].

The major complication in the computation of these radial couplings is the accurate treatment of the neutron-target interactions. These terms are genuinely four-body-like in that they involve and couple the three coordinates \mathbf{R} , $\boldsymbol{\rho}$ and \mathbf{r} . We use the generalised multipole expansion of [6]. Since the coupled equations solutions are needed for ρ and r values spanning the entire ^{22}C ground-state, we note that accurate calculations of the multipole coupling potentials, $V_{k_R k_\rho k_r}(R, \rho, r)$, require the use of different techniques for small values (Gaussian expansion) and larger values (direct numerical integration) of r and ρ (readers are referred to Appendix A of Ref. [6]). The result, from the solution of this set of R -dependent coupled channels equations, is an (ρ, r) -dependent reaction matrix, $M_{\alpha';\alpha}^J(\rho, r)$, for the amplitudes of the outgoing waves in each included final-state configuration α' , as

computed from the asymptotic ($R \rightarrow \infty$) forms of the coupled channels radial functions

$$\chi_{\alpha'\alpha}^J(R, \rho, r) \rightarrow F_L(KR) \delta_{\alpha'\alpha} + M_{\alpha';\alpha}^J(\rho, r) H_L^+(KR).$$

The physical elastic or breakup amplitudes are now determined by evaluating the integrals over ρ and r of these adiabatic, (ρ, r) -dependent amplitudes $M_{\alpha';\alpha}^J$ weighted by the probability amplitudes for finding the $^{20}\text{C}+n+n$ system with each given (ρ, r) in the entrance and exit channels, i.e. by the radial wave functions $U_{[\beta S]I}(\rho, r)$. That is,

$$\mathcal{M}_{\alpha';\alpha}^{SJI'I} = \int d\rho \int dr U_{[\beta' S]I'}^*(\rho, r) M_{\alpha';\alpha}^J(\rho, r) U_{[\beta S]I}(\rho, r).$$

The relationship of these \mathcal{M} to the usual partial wave transition amplitudes, where the physical total angular momentum of the system is \mathcal{J} , having couplings $[J S] \mathcal{J}$ and $[L I] \mathcal{J}$, is then, with $\hat{k} = \sqrt{2k+1}$ etc.,

$$T_{L'I';LI}^{\mathcal{J}} = \sum_{\ell_1 \ell_2 \mathcal{L} \ell'_1 \ell'_2 \mathcal{L}' S J k} (-)^{\phi} \hat{k} \hat{J} \hat{I} \hat{I}' W(\mathcal{L} \mathcal{L}' \mathcal{L}' L', Jk) W(I \mathcal{L}' I' \mathcal{L}', S k) W(L L' I I', k \mathcal{J}) \mathcal{M}_{\alpha';\alpha}^{SJI'I}, \quad (4)$$

where the phase is $\phi = L+L'-J+S+I-I'+\mathcal{L}+\mathcal{L}'-\mathcal{J}-k$.

The elastic scattering amplitudes have $I = I'$ and involve

only those channels, $[[\ell_1 \ell_2] \mathcal{L} S] I$, that enter the projectile ground state wave function, Eq. (1).

This general angular momentum coupling structure simplifies significantly when discussing the elastic T-matrix for ^{22}C scattering, with $I^\pi = 0^+$. The Racah coefficients in Eq. (4) then require $k = 0$, $\mathcal{J} = L = L'$, and $\mathcal{L} = \mathcal{L}' = S$ for all of the included ground state contributions. Thus, the T-matrix elements reduce to simplified sums over the most important ground state components. Defining $T^\mathcal{J} \equiv T_{\mathcal{J}0; \mathcal{J}0}^\mathcal{J}$ then

$$T^\mathcal{J} = \sum_{\ell_1 \ell_2 \ell'_1 \ell'_2 JS} \left(\frac{\hat{J}}{\hat{S}\hat{\mathcal{J}}} \right)^2 \mathcal{M}_{\{[\ell'_1 \ell'_2] S, \mathcal{J}\}; \{[\ell_1 \ell_2] S, \mathcal{J}\}}^{S, J00}. \quad (5)$$

From these one obtains the elastic S-matrix elements, $S_{22}^\mathcal{J} = 1 + 2iT^\mathcal{J}$, and hence the coupled-channels model reaction cross sections

$$\sigma_R = \frac{\pi}{K^2} \sum_{\mathcal{J}} \hat{\mathcal{J}}^2 (1 - |S_{22}^\mathcal{J}|^2). \quad (6)$$

B. Eikonal four-body model calculations

The four-body adiabatic model Schrödinger equation, Eq. (3), can also be solved more simply, but more approximately, by use of the eikonal/Glauber approximation – that the scattering of the projectile and its constituents is forward focussed and involves negligible longitudinal (beam directional) momentum transfers. The formalism and applications of this technique to reaction cross section calculations for weakly-bound three-body projectiles has been presented in Refs. [1, 2] and references therein. Here we summarize the essential re-

sults and the major differences from the coupled channels methodology of the previous subsection.

Now, the (semi-classical) elastic scattering channel S-matrix of the projectile, expressed as a function of the impact parameter b of its center-of-mass, is more simply calculated, based on the eikonal elastic S-matrices for the independent scattering of its constituent neutrons and core nucleus from the target, as

$$\mathcal{S}_{22}(b) = \int d^2\boldsymbol{\sigma} \int d^2\mathbf{s} \xi(\boldsymbol{\sigma}, \mathbf{s}) \mathcal{S}_{20}(b_{20}) \mathcal{S}_{n1}(b_1) \mathcal{S}_{n2}(b_2).$$

Here $\boldsymbol{\sigma}$ and \mathbf{s} are the components of the $^{20}\text{C}+n+n$ relative coordinates $\boldsymbol{\rho}$ and \mathbf{r} in the impact parameter plane of the reaction, the plane normal to the incident beam direction. The Glauber approach thus avoids the requirement for coupled channels solutions and is computationally very economical. The individual S-matrices \mathcal{S}_{n1} ($= \mathcal{S}_{n2}$) and \mathcal{S}_{20} should be calculated from the same neutron- and core-target complex optical interactions, V_n and V_{20} , used in the coupled channels calculations.

The projectile ground-state wave function now enters the calculations through the z -direction-integrated probability density of the projectile, $\xi(\boldsymbol{\sigma}, \mathbf{s})$, sometimes referred to as the projectile thickness function,

$$\xi(\boldsymbol{\sigma}, \mathbf{s}) = \int_{-\infty}^{\infty} d\rho_3 \int_{-\infty}^{\infty} dr_3 \langle |\Phi_{00}(\boldsymbol{\rho}, \mathbf{r})|^2 \rangle_{\text{spin}} \quad (7)$$

where $\Phi_{00}(\boldsymbol{\rho}, \mathbf{r})$ is the ^{22}C ground state wave function (with $IM_I = 00$) and ρ_3 and r_3 are the beam direction (z -components) of $\boldsymbol{\rho}$ and \mathbf{r} . The relevant $^{20}\text{C}+n+n$ position probability density is summed over the neutron spin variables. More explicitly, for the $IM_I = 00$ case of Eq. (1), when $\mathcal{L} = S$, we are required to calculate

$$\begin{aligned} \langle |\Phi_{00}(\boldsymbol{\rho}, \mathbf{r})|^2 \rangle_{\text{spin}} &= \frac{1}{(4\pi)^2} \sum_{\ell_1 \ell'_1 \ell_2 \ell'_2 \mathcal{L} \Lambda} (-)^{\mathcal{L}+\Lambda} \hat{\ell}_1 \hat{\ell}'_1 \hat{\ell}_2 \hat{\ell}'_2 \hat{\Lambda}^2 W(\ell_1 \ell_2 \ell'_1 \ell'_2; \mathcal{L} \Lambda) P_\Lambda(\cos \gamma) \\ &\times \begin{pmatrix} \ell_1 & \ell'_1 & \Lambda \\ 0 & 0 & 0 \end{pmatrix} \begin{pmatrix} \ell_2 & \ell'_2 & \Lambda \\ 0 & 0 & 0 \end{pmatrix} \frac{U_{[[\ell_1 \ell_2] \mathcal{L} \mathcal{L}]0}(\rho, r)}{\rho r} \times \frac{U_{[[\ell'_1 \ell'_2] \mathcal{L} \mathcal{L}]0}(\rho, r)}{\rho r} \end{aligned} \quad (8)$$

where $P_\Lambda(\cos \gamma)$ is the Legendre Polynomial and γ is the angle between vectors $\boldsymbol{\rho}$ and \mathbf{r} . Thus the different angular momentum components in the projectile ground-state enter explicitly here. The evaluations of the z -directional integrals in Eq. (7) for $\xi(\boldsymbol{\sigma}, \mathbf{s})$ use the generalisation of the scheme outlined in Ref. [21] for the higher orbital angular momentum components ℓ_1 and ℓ_2 that are needed here.

C. Reaction model inputs

We perform calculations for ^{22}C incident on a ^{12}C target at 300 MeV per nucleon. The neutron- and ^{20}C core-target interactions were calculated using the single-folding $t_{NN}\rho_t$ model (for the nucleon-target system) and double-folding $t_{NN}\rho_c\rho_t$ models (for the core-target system). The inputs needed were the point neutron and proton one-body densities for the core (c) and target (t) nuclei and an effective nucleon-nucleon (NN) interaction t_{NN} . The ^{20}C density was taken from a spherical

Skyrme (SkX interaction [20]) HF calculation. The density of the carbon target was taken to be of Gaussian form with a point-nucleon root-mean-squared radius of 2.32 fm. A zero-range NN effective interaction was used. Its strength was calculated from the free neutron-neutron and neutron-proton cross sections at the beam energy and the ratio of the real-to-imaginary parts of the forward scattering NN amplitudes, at 300 MeV, were interpolated (using a polynomial fit) from the values tabulated from the nucleon-nucleus analysis of Ray [22]. We note that the use of these folded neutron- and core-target interactions provided a good description of the recent neutron-removal data from the heavy carbon isotopes at 250 MeV/nucleon [5]. The recent analysis by Bertulani and De Conti [23] also suggests that further corrections to this procedure, due to additional Pauli blocking corrections to the NN effective interaction in the core-target system, should be very small at the energies of interest here.

Some numerical details of these extended adiabatic model calculations are as follows. The calculations used an extensively modified version of the code ADO developed for the earlier work of Christley *et al.* [6]. We use a 24×24 (Gauss-Legendre quadrature) grid of (ρ, r) values on the interval $[0, 24]$ fm, with 12 points on $[0, 10]$ fm and 12 points on $[10, 24]$ fm for both ρ and r . The time-consuming, four-body neutron-target multipole coupling potentials $V_{k_R k_\rho k_r}(R, \rho, r)$ are pre-calculated and read back for each (ρ, r) coupled channels solution. Calculations are carried out for R values of $[0, 30]$ fm (with step 0.005 fm) and 500 partial waves were found to be adequate for calculations of the entire elastic S-matrix. Calculations where every partial wave was computed were well reproduced when interpolating the (smooth) S-matrix every 10th partial wave. The specific breakup configurations in the coupled channels sets, and projectile ground-state components used, are discussed in the next section. To allow fair comparisons, calculations using the Glauber few-body approach used consistent wave function and interactions inputs, with impact parameters on the range $[0, 30]$ fm.

D. Reaction cross section results

The coupled-channels adiabatic calculations were performed when including several combinations of ground-state and core+n+n elastic breakup continuum configurations, $\delta \equiv [[\ell_1 \ell_2] \mathcal{L} S] I$ (see also Fig. 1), to assess the importance of the different breakup configurations and the convergence of the calculations. Since the ^{22}C ground state has spin $I^\pi = 0^+$, all ground state configurations have $\mathcal{L} = S$ (where $[s_1 s_2] S$) and, in general, $S = 0$ or 1. However, the computed three-body wave functions of Table I actually contain negligible spin $S = 1$ components, in total less than 1.5% of the full wave function normalization, and these small fragments are not included. Since, when assuming central nucleon- and ^{20}C -target interac-

tions, the S is a good quantum number of the coupled channels equations, the elastic amplitudes of Eq. (5) involve only $S = 0$ channels.

The ^{22}C reaction cross sections on a carbon target are calculated for the different wave functions of subsection II B, that are summarised in Table I. The resulting cross sections are shown in Table II and in Figure 2, there as a function of the rms radius of the ^{22}C ground state. To assess the convergence of the calculations with the breakup model space different numbers of the δ configurations are used, shown as different $\sigma_R(i)$, $i = a, b, c, d$ and Ad, each including successively more (coupled) angular momentum configurations. Calculations (a) (red diamond symbols) include only the $[[00]00]0$ configuration, the dominant component (70–77%, see Table I) of the ground-state wave function. Calculations (b) (green inverted triangles) also include the next most important $[[22]00]0$ configuration, that comprises 24–17% of the ground state. So, calculations (a) and (b) include the major parts of the ground state wave function plus the coupling to breakup channels with these angular momenta. The next largest component of the calculated ground state wave functions (4–5%) has the $[[44]00]0$ structure, see below, while a remaining $\approx 1.5\%$ is distributed over many small $S = 1$ fragments, as was discussed above. The importance of this $[[44]00]0$ ground/breakup state term is discussed below. Calculations (c), (d) and (Ad) result as we incrementally expand the breakup model space by adding the couplings to: (c) $[[01]10]1$ (blue triangles), (d) $[[02]20]2$ and $[[20]20]2$ (open squares), and finally (Ad) the $[[22]20]2$ (black diamonds) breakup configurations. The latter two calculations essentially coincide on the figure having cross sections that differ by less than 2 mb. Figure 2 shows the reduced importance of the channels involving increasing orbital angular momentum transfers among the projectile constituents. The inclusion of the $\delta = [[44]00]0$ ground-state and breakup configuration affected the calculated cross sections (for wave functions k1 and k2) by less than 0.1 mb and was not considered further.

It should be noted that the overall ^{22}C ground state wave function was (re)normalized to unity for each subset of the $[[00]00]0$, $[[22]00]0$ and $[[44]00]0$ ground-state configurations included in these results. We also note that *all* of the calculations shown here include projectile breakup effects, each to a different degree, so, although sharing some visual similarities, the comparisons shown in Figure 2 are different to the no-breakup versus breakup calculation comparisons made for example in Refs. [1, 2].

Calculations were also carried out using the eikonal (Glauber) few-body approach as outlined in section III B. For consistency and fair comparison with the coupled channels adiabatic approach, these calculations included the same dominant $[[00]00]0$ and $[[22]00]0$ configurations of the calculated ground state wave functions. The cross sections obtained are shown in Table II, as $\sigma_R(\text{Gl})$, and in Figure 2 (black filled squares). The dependence of the results on the ^{22}C rms radius are seen to track those

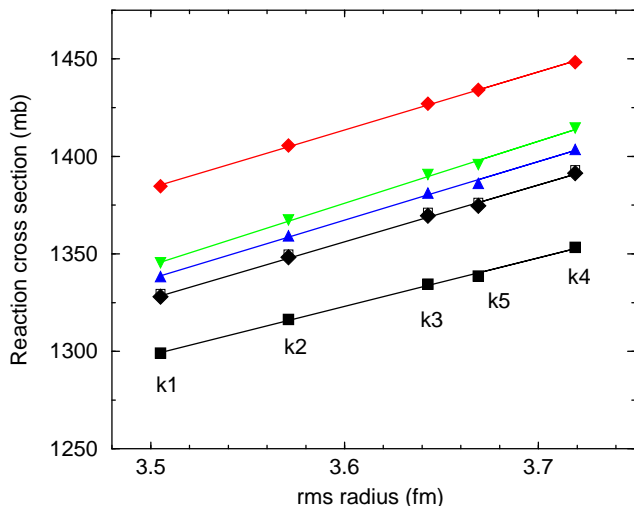


FIG. 2: (Color online) Calculated reaction cross sections, for ^{22}C on a carbon target at 300 MeV per nucleon, as a function of the rms radii of the ^{22}C three-body model wave functions. The different adiabatic model calculations, $\sigma_R(a)$ through $\sigma_R(\text{Ad})$, that systematically increase the breakup model space are described in the text. The black diamonds show the results of the most complete adiabatic model calculation $\sigma_R(\text{Ad})$. The black filled squares show the results for the four-body Glauber model calculations, $\sigma_R(\text{Gl})$, for the same three-body wave functions, that include the $[[00]00]0$ and $[[22]00]0$ ground state wave function components in common with the adiabatic calculations.

TABLE II: Calculated reaction cross sections for ^{22}C , incident on a carbon target at 300 MeV per nucleon, for the three-body model wave functions k1–k5 presented in Table I. The different intermediate, (a), (b), (c), (d) and final (Ad) adiabatic model and the Glauber few-body model (Gl) cross sections are discussed in the text.

Model	k1	k2	k3	k4	k5
E_{3B} (MeV)	-0.442	-0.294	-0.163	-0.046	-0.134
$\sigma_R(a)$ (mb)	1384.6	1405.6	1427.0	1448.3	1434.1
$\sigma_R(b)$ (mb)	1345.4	1367.4	1390.7	1414.5	1395.7
$\sigma_R(c)$ (mb)	1338.3	1359.2	1381.2	1403.6	1386.1
$\sigma_R(d)$ (mb)	1329.5	1349.8	1371.1	1392.9	1376.2
$\sigma_R(\text{Ad})$ (mb)	1328.0	1348.3	1369.6	1391.3	1374.6
$\sigma_R(\text{Gl})$ (mb)	1299.1	1316.3	1334.5	1353.3	1338.6

of the coupled channels equations but the magnitudes of the cross sections are consistently smaller, by $\approx 2\%$, than those of the final, most complete $\sigma_R(\text{Ad})$ calculations. This level of agreement provides a benchmark of the accuracy of the Glauber few-body approach at an energy of 300 MeV/nucleon, which is valuable given the relative computational efficiency of the method. We also note that, unlike the coupled channels adiabatic calcu-

lations, there is no explicit truncation of the breakup channels model space used in the eikonal/Glauber approach, although, based on the observed convergence of the adiabatic calculations, Figure 2, we do not believe that this is the source of the small differences observed. The eikonal/Glauber approach also includes a more approximate treatment of the reaction dynamics, (i) based on the eikonal elastic S-matrices, \mathcal{S}_n and \mathcal{S}_{20} , that are calculated from the neutron- and ^{20}C -target optical potentials assuming straight line paths through the interaction region, and (ii) assuming there is no longitudinal momentum transfer in the collisions with the target. Thus, the calculated cross sections show both the convergence of the adiabatic model calculations and quantify the small differences between the adiabatic and adiabatic+eikonal dynamical treatments on the calculated projectile-target absorption ($1 - |\mathcal{S}_{22}|^2$) and reaction cross section calculations for the ^{22}C -target system at the energies of interest here. These differences may of course be more significant, quantitatively, for other more exclusive observables and will be clarified in future work in this direction.

IV. SUMMARY

We have presented converged coupled channels adiabatic four-body reaction model calculations (using a three-body structure model) of the reaction cross sections for the last particle-bound carbon isotope ^{22}C , at intermediate energy. The coupled channels-based calculations of this work are compared with Glauber few-body model calculations, that make the additional eikonal approximation in the solution of the adiabatic Schrödinger equation. A set of model three-body wave functions were obtained, all of which have reasonable two-neutron separation energies S_{2n} , and which have different values for the scattering length a_0 for the assumed virtual $2s_{1/2}$ -state in the unbound $n+^{20}\text{C}$ two-body subsystem. We have detailed the formulation of the ^{22}C elastic scattering S-matrix from which we calculate the reaction cross sections. The calculations presented include s -, p - and d -wave four-body breakup channels. g -wave effects were found to be negligible. The approach used is well-suited to the energy of the present study, 300 MeV per nucleon, and the calculations reveal the degree of sensitivity of the reaction cross sections to the assumed structure of the projectile, in particular its rms radius. Compared to calculations for lighter nuclei, the range of rms radii from the different ^{22}C three-body structures is relatively small with a corresponding smaller cross section sensitivity. Comparisons of these coupled channels adiabatic results with four-body Glauber model calculations, based on the same three-body wave functions and neutron- and ^{20}C -target interactions, agree to within 2%.

The approach is relevant to current and future experimental programmes at fragmentation-based RIB facilities, such as RIBF, FRIB and GSI/FAIR. The present analysis reveals the high precision of experimental reac-

tion cross section data that is needed to interrogate the ^{22}C structure and the breakup reaction dynamics, pointing to the likely advantage of more exclusive observables.

Acknowledgments

This work was supported by a TÜBİTAK BİDEB-2219 Postdoctoral Research Fellowship (for YK) and by the

UK Science and Technology Facilities Council (STFC) (for JAT) under Grant ST/J000051. The authors thank Professor Ian Thompson and Dr Natalia Timofeyuk for advice on the implementations of the computer codes EFADDY and POLER.

-
- [1] J. S. Al-Khalili and J. A. Tostevin, *Phys. Rev. Lett.* **76**, 3903 (1996).
 - [2] J. S. Al-Khalili, J. A. Tostevin, and I. J. Thompson, *Phys. Rev. C* **54**, 1843 (1996).
 - [3] K. Tanaka *et al*, *Phys. Rev. Lett.* **104**, 062701 (2010).
 - [4] Takashi Nakamura, *J. Phys.: Conf. Ser.* **381**, 012014 (2012).
 - [5] N. Kobayashi *et al*, *Phys. Rev. C* **86**, 054604 (2012).
 - [6] J. A. Christley, J. S. Al-Khalili, J. A. Tostevin, and R. C. Johnson, *Nucl. Phys.* **A624**, 275 (1997).
 - [7] T. Matsumoto, E. Hiyama, K. Ogata, Y. Iseri, M. Kamimura, S. Chiba, and M. Yahiro, *Phys. Rev. C* **70**, 061601(R) (2004).
 - [8] M. Rodriguez-Gallardo, J.M. Arias, J. Gómez-Camacho, R. C. Johnson, A.M. Moro, I.J. Thompson, and J.A. Tostevin, *Phys. Rev. C* **77**, 064609 (2008); M. Rodriguez-Gallardo, J.M. Arias, J. Gómez-Camacho, A.M. Moro, I.J. Thompson, and J.A. Tostevin, *Phys. Rev. C* **80**, 051601(R) (2009).
 - [9] EFADDY Faddeev Bound State program, I. J. Thompson, V. D. Efros, and F. Nunes; Available at: <http://www.fresco.org.uk/programs/efaddy/index.html>
 - [10] Y. Kucuk and J. A. Tostevin, *J. Phys.: Conf. Series* **381** 012109 (2012).
 - [11] G. Audi and A. H. Wapstra, *Nucl. Phys.* **A729**, 337 (2003).
 - [12] L. Gaudefroy *et al*, *Phys. Rev. Lett.* **109**, 202503 (2012).
 - [13] S. Mosby *et al*, *Nucl. Phys.* **A909**, 69 (2013).
 - [14] W. Horiuchi and Y. Suzuki, *Phys. Rev. C* **74**, 034311 (2006).
 - [15] M. T. Yamashita, R. S. Marques de Carvalho, T. Frederico, and Tomiod Lauro, *Phys. Lett.* **B697**, 90 (2011).
 - [16] D. Gogny, P. Pires, and R. De Tourreil, *Phys. Lett.* **B32**, 591 (1970).
 - [17] F. D. Becchetti, Jr. and G. W. Greenlees, *Phys. Rev.* **182**, 1190 (1969).
 - [18] POLER Complex energy S-matrix pole search program, I. J. Thompson, private communication
 - [19] J. Bang, B. Danilin, V. D. Efros, J. S. Vaagen, M.V. Zhukov, and I. J. Thompson, *Physics Reports* **264**, 27 (1996).
 - [20] B. A. Brown, *Phys. Rev. C* **58**, 220 (1998).
 - [21] J.S. Al-Khalili, I.J. Thompson and J.A. Tostevin, *Nucl. Phys.* **A581**, 331 (1995).
 - [22] L. Ray, *Phys. Rev. C* **20**, 1857 (1979).
 - [23] C. A. Bertulani and C. De Conti, *Phys. Rev. C* **81**, 064603 (2010).